RESEARCH PAPER

PCCP
www.rsc.org/pccp

Isothermal activation of $Mo_2O_5^{2+}$–ZSM-5 precursors during methane reactions: effects of reaction products on structural evolution and catalytic properties

Howard S. Lacheen and Enrique Iglesia*

Department of Chemical Engineering, University of California at Berkeley, Berkeley, CA 94720, USA. E-mail: iglesia@cchem.berkeley.edu

Received 30th September 2004, Accepted 4th November 2004
First published as an Advance Article on the web 22nd December 2004

The dynamics of carburization of Mo-oxo precursors exchanged onto H–ZSM-5 strongly influence initial induction periods and steady-state rates during catalytic pyrolysis of CH_4 to alkenes and arenes at 900–1000 K. The effects of co-reactants and of activating conditions were examined by on-line time-resolved mass spectrometric analysis of effluent streams using rigorous analyses to account for equilibrium effects on measured rates. Ethene co-reactants and the larger hydrocarbons to which it converts on acid sites in H–ZSM-5 led to much faster carburization of exchanged $(Mo_2O_5)^{5+}$ dimers and to shorter induction periods than with pure CH_4 reactants, but steady-state pyrolysis rates were unchanged, indicating that CH_4 and C_2H_4 form similar MoC_x clusters during carburization of exchanged Mo-oxo precursors. H_2 treatment at 973 K before CH_4 reactions led to reduction of Mo^{6+} species to Mo^{4+}, which carburize faster than $(Mo_2O_5)^{5+}$ precursors during initial contact with CH_4. This H_2 pretreatment or the use of CH_4–H_2 reactant mixtures did not influence steady-state pyrolysis rates, once contributions from reverse reactions were taken into account. With pure CH_4 streams, $(Mo_2O_5)^{5+}$–ZSM-5 converts to active MoC_x clusters within zeolite channels *via* autocatalytic processes, in which higher hydrocarbons, initially formed during initial conversion of MoO_x to MoC_x structures, lead to faster carburization of downstream catalyst sections. Concurrently, H_2O and CO_2 formed during this incipient carburization of exchanged $(Mo_2O_5)^{5+}$ and unexchanged MoO_3 present in trace amounts inhibit and even prevent carburization and lengthen activation periods. Activation protocols with C_2H_4 were also successful in the activation of more refractory high-valent metal-oxo species, such as WO_x and VO_x, exchanged onto H–ZSM-5. The formation of active carbide structures occurred in less than 300 s, instead of 4 ks and 16 ks for VO_x and WO_x samples, respectively, in pure CH_4 reactants. These activation protocols led to VC_x–ZSM5 catalysts about three times more active than those activated in pure CH_4 reactants.

1. Introduction

The conversion of remote natural gas to petrochemicals and liquid fuels and chemicals remains a formidable technological challenge.[1] Exchanged cations within medium-pore pentasil zeolites act as precursors that activate *in situ* to form carbide clusters; these carbide clusters catalyze non-oxidative reactions of CH_4 to form alkenes, benzene, and polynuclear arenes at high temperatures ($\sim$1000 K).[2–5] Mo, V, Ti and W have been exchanged into ZSM-5 to varying degrees and the resulting materials catalyze these reactions.[6–9] Mo–ZSM-5 and W–ZSM-5 remain the most active reported catalysts; they lead to near-equilibrium CH_4 conversion to ethane, ethene and benzene with remarkable catalyst stability, even at the severe conditions required for significant equilibrium conversions in endothermic CH_4 pyrolysis reactions.[10,11]

Mo^{6+} exchange occurs *via* migration of volatile $(MoO_3)_n$ species during thermal treatment of MoO_3/H–ZSM-5 samples prepared by impregnation with aqueous solutions or by physical mixing of MoO_3 and ZSM-5 powders. $(Mo_2O_5)^{2+}$ dimers bridging two exchange sites form during these processes and undergo stoichiometric reduction and carburization to form MoC_x clusters during initial contact with CH_4 reactants at $\sim$1000 K.[12,13] The presence and catalytic involvement of these MoC_x clusters were confirmed by measuring the evolution of CO, CO_2 and H_2O during an induction period, in which catalysis becomes detectable and reaches steady-state rates as oxygen atoms are gradually removed from the exchanged MoO_x precursors.[14] The evolution of Mo carbide structures during the initial stages of contact with CH_4 was detected by X-ray absorption spectra during reaction[15] and confirmed by X-ray photoelectron spectroscopy after reaction.[11,16] Mo_2C structures are stable during CH_4 pyrolysis and resist sintering because of their high melting point and low vapor pressure.[17] The three-dimensional network of ten-ring channels (0.51–0.55 nm) in ZSM-5 provides Brønsted acid sites, which catalyze chain growth, within a constrained environment that also contains MoC_x clusters and which inhibits the formation of large condensed arene rings and the agglomeration of active MoC_x species. Similar structural evolution and catalytic requirements have been established for CH_4 reactions on W/ZSM-5 materials.[10]

Even after considerable effort, the detailed structure of MoO_x precursors and of active MoC_x species and the role of the CO, H_2, CO_2 and H_2O initially formed on carburization and activation rates remain controversial. $(Mo_2O_5)^{2+}$–ZSM-5 reduces and carburizes at rates that increase with time after an initial induction period; slow CH_4 activation on $(Mo_2O_5)^{2+}$ dimers causes incipient reduction, but also the concurrent formation of possibly more effective reductants, such as CO and H_2.[13,18] As O-atoms are removed and H_2 or CO form, the remaining oxides downstream may reduce more rapidly until oxygen is depleted and the resulting stoichiometric carbides catalyze hydrocarbon synthesis. Hydrocarbons formed during the early stages of activation can also act as reduction and carburization agents for Mo-oxo precursors downstream.

DOI: 10.1039/b415166f

Ha *et al.*[19] detected C_2H_2 and C_2H_4 during CH_4 reactions on Mo/ZSM-5 and suggested that C_2H_2 acts as an intermediate in arene formation. Carburization rates of MoO_x clusters in alkane/H_2 mixtures are known to increase with alkane chain size;[20] thus, C_{2+} species that form as $(Mo_2O_5)^{2+}$–ZSM-5 carburizes may increase activation rates as these initial products make contact with the rest of the catalyst bed.

Here, we examine the effects of reactant stream composition on activation rates and on the structure and catalytic reactivity of the MoC_x clusters formed during activation in an effort to design activation protocols that lead to more active, selective, or stable CH_4 pyrolysis catalysts. We exploit methods for fast chemical analysis of product streams ($\sim$1 s) using on-line mass spectrometry to measure the dynamics of $(Mo_2O_5)^{2+}$–ZSM-5 activation using H_2, H_2O, CO_x or C_2H_4 with CH_4 reactants. In the process, we examine effects of residence time and of CH_4 and co-reactant concentrations on carburization rates and propose a consistent "mechanism" for catalyst activation in CH_4. We also report similar activation pathways and protocols for WO_x–ZSM-5 and VO_x–ZSM-5 samples using C_2H_4/CH_4, which lead to faster activation on both samples and to higher steady-state CH_4 pyrolysis rates than for VO_x–ZSM-5 activated in pure CH_4 reactants.

2. Experimental apparatus and procedure

2.1 Synthesis of exchanged MoO_x/H–ZSM-5

H–ZSM-5 was prepared by controlled removal of the organic template from Na–ZSM-5 ($Si/Al_f = 20$, Zeochem). Na–ZSM-5 (2 g) was placed within a quartz tube (2 cm diameter) and held in place by quartz wool. Samples were heated to 823 K at 0.083 K s^{-1} in He (2.5 cm^3 s^{-1} g^{-1} Airgas, UHP). The flow was switched to air (2.5 cm^3 s^{-1} g^{-1} Airgas, zero grade) for 2 h and the samples were then cooled to ambient temperature in He. Na^+ cations were replaced with NH_4^+ by contacting Na–ZSM-5 (10 g) three times with 1 L fresh NH_4NO_3 solutions (1 M, Fisher, Cert. ACS, in deionized H_2O) at 353 K for 12 h. The resulting NH_4–ZSM-5 was washed with 2 L deionized water and dried for 12 h at 400 K in ambient air. H–ZSM-5 was formed by subsequent treatment in dry air (1.67 cm^3 s^{-1} g^{-1}) at 773 K for 24 h using a heating rate of 0.167 K s^{-1}.

Exchanged MoO_x-H–ZSM-5 samples were prepared by grinding a physical mixture of MoO_3 (Johnson Matthey, 99.5%) and H–ZSM-5 for $\sim$0.2 h using an agate mortar and pestle to form intimate composites with Mo/Al_f ratios of 0.25 and 0.41. These mixtures were heated to 623 K at 0.167 K s^{-1} and held at this temperature for 24 h in 20% O_2/He (1.67 cm^3 s^{-1}, Matheson, UHP). The sample temperature was then increased to 973 K at 0.167 K s^{-1} and held for 2 h at 973 K in the same stream. This thermal treatment led to the formation of $Mo_2O_5^{2+}$ dimers by replacement of two protons and concurrent evolution of H_2O.[12,13] The exchanged $(Mo_2O_5)^{2+}$–ZSM-5 material was pressed into pellets and sieved to retain aggregates with 0.12–0.25 mm diameter, which were used in all catalytic experiments.

2.2 Synthesis of WO_x/H– and VO_x/H–ZSM-5

WO_x/H–ZSM-5 was prepared from WCl_6 (Aldrich, 99.9+%) and H–ZSM-5 mixtures using previously reported procedures.[10] H–ZSM-5 (2 g) was evacuated to $<$0.13 Pa in an ampoule and dehydrated by heating to 573 K at 0.17 K s^{-1} and maintained at 573 K for 1 h. WCl_6 was then transferred into the ampoule to give a W/Al_f ratio of 0.25 and the ampoule was sealed and heated to 623 K at 0.17 K s^{-1} and held at 623 K for 5 h before cooling to ambient temperature. The contents of the ampoule were transferred into a quartz fritted U-tube reactor under nitrogen. WCl_x–ZSM-5 samples (0.5 g) were heated to 373 K at 0.17 K s^{-1} in 1 cm^3 s^{-1} He. The feed was then changed to 1 cm^3 s^{-1} 20 kPa O_2/0.5 kPa H_2O/81 kPa He and heated to 623 K at 0.17 K s^{-1}. H_2O was added by passing 20% O_2/He through a bubbler held at 273 K within an ice bath. The bubbler was then bypassed and the reactor was heated to 973 K at 0.17 K s^{-1} and held at 973 K for 1 h. VO_x–ZSM-5 ($V/Al_f = 0.2$) was prepared using the above procedure but using $VOCl_3$ (Aldrich, 99.995%) and heating the sealed ampoule to 473 K instead of 623 K.

2.3 Catalytic CH_4 pyrolysis rates and selectivities

Catalysts (0.3 g, Mo/Al_f = 0.25–0.41) were exposed to CH_4-containing streams at 950 K in a fritted quartz reactor (8 mm diameter). Stream compositions and flow rates were set by electronic mass flow controllers (Porter Instruments, Model 201); all reactants were ultra-high purity gases (Matheson). H_2O was added to flowing streams by passing 5% H_2/Ar over CuO (Aldrich, 13 wt.% Cu/Al_2O_3) at 673 K at the flow rate required to produce the desired H_2O molar rate by stoichiometric reduction of CuO.

Product formation rates were measured by on-line mass spectrometry (MKS Minilab) using an atmospheric sampling system equipped with a heated capillary. Overlapping mass fragments in complex product mixtures were deconvoluted using methods adapted from previous studies[14] to measure individual concentrations after calibrating fragmentation patterns and detector response (relative to He) using pure species (details in Appendix). Concentrations measured by on-line mass spectrometry at 1 s time intervals agreed with those measured less frequently ($\sim$0.4 h) by gas chromatography (Agilent 6890). Hydrocarbons were separated using a capillary column (Agilent HP-1, 50 m $\times$ 0.32 mm $\times$ 1.05 μm film) and detected using flame ionization. CH_4, H_2, CO, Ar, CO_2 and H_2O were separated in a packed column (Agilent Poropak Q, 4.5 m) and detected by thermal conductivity. Detection limits were 50 ppm and 1 ppm for thermal conductivity and flame ionization detection, respectively.[13]

Product formation rates (mol [product formed] g-atom Mo^{-1} s^{-1} are reported as measured net rates or forward rates. Forward rates, $r_{forward}$, are obtained from measured rates, r_{net}, using:

$$r_{net} = r_{forward}(1 - \eta) \quad (1)$$

where the approach to equilibrium, η (*e.g.*, eqn. (2), for benzene formation from methane) is given in terms of the partial pressures, p_i, of chemical species, i, and the equilibrium constant, K, for each reaction.[21]

$$\eta = \frac{p_{C_6H_6}^{1/6} p_{H_2}^{3/2}}{p_{CH_4} K} \quad (2)$$

3. Results and discussion

3.1 Transient changes in structure and composition during exposure of $(Mo_2O_5)^{2+}$–ZSM-5 to CH_4

Baseline data for experimental comparisons among various reactant mixtures were obtained by exposing $(Mo_2O_5)^{2+}$–ZSM-5 ($Mo/Al_f = 0.41$) to a Ar : CH_4 : He mixture (1 : 9 : 45; 101.3 kPa) at 950 K. H_2, C_2H_4, C_2H_6, C_6H_6, C_7H_8 and $C_{10}H_{12}$ were the most abundant products detected by gas chromatography, and rates and selectivities were similar to those previously reported on a catalyst of similar composition and prepared by the same methods.[13,22] C_2H_2 was not detected at any time, in contrast with reports by Ha *et al.* for CH_4 reactions on Mo–ZSM-5 at 1023 K,[19] possibly because of more favorable thermodynamics at the higher temperatures in the previous study[23], and its role as a reactive intermediate in arene formation remains uncertain. In contrast, C_2H_4 was detected at all CH_4 conversions, and it is involved as an intermediate in the

synthesis of arene products.[15] In view of its presence and presumed intermediacy, C_2H_4 was chosen as a co-reactant to explore its effect in the transient evolution of catalytic activity during activation and to compare the effects of reductants with different carbon chain length.

Product formation rates are shown in Fig. 1a as a function of time during initial contact with $Ar/CH_4/He$ mixtures at 950 K. Only CO, CO_2, H_2O and H_2 were detected during the first 600 s, and H_2O and CO formation rates were initially similar (5×10^{-4} mol g-atom Mo^{-1} s^{-1}). H_2O and CO_2 formation rates decreased monotonically with time, but CO formation rates increased sharply with time on stream (to a maximum value of 6×10^{-3} mol g-atom Mo^{-1} s^{-1}). A momentary increase in H_2O formation rates was observed slightly before this maximum CO formation rate, but H_2O formation rates were $\sim$10 times lower than CO formation rates; the implications of this water evolution will be discussed later in the context of the kinetic effects of H_2O on activation rates. Hydrocarbons (*e.g.* benzene; Fig. 1a) were not detected initially, but their formation rates increased as MoO_x precursors reduced and carburized;[12,14] we denote this elapsed time between contact with reactants and the incipient formation of pyrolysis products (defined by the spectrometer detection limit of $\sim 10^{-3}$ kPa C_6H_6) as the induction period. Benzene, the most abundant product during steady-state catalysis, first appeared $\sim$600 s after introducing pure CH_4 reactants (Fig. 1a) and its formation rate then increased sharply to its steady-state value of 4.0×10^{-4} mol C_6H_6 g-atom Mo^{-1} s^{-1}; hydrocarbon formation rates ultimately decreased slowly with time as a result of catalyst deactivation caused by the formation of unreactive carbon residues.[24]

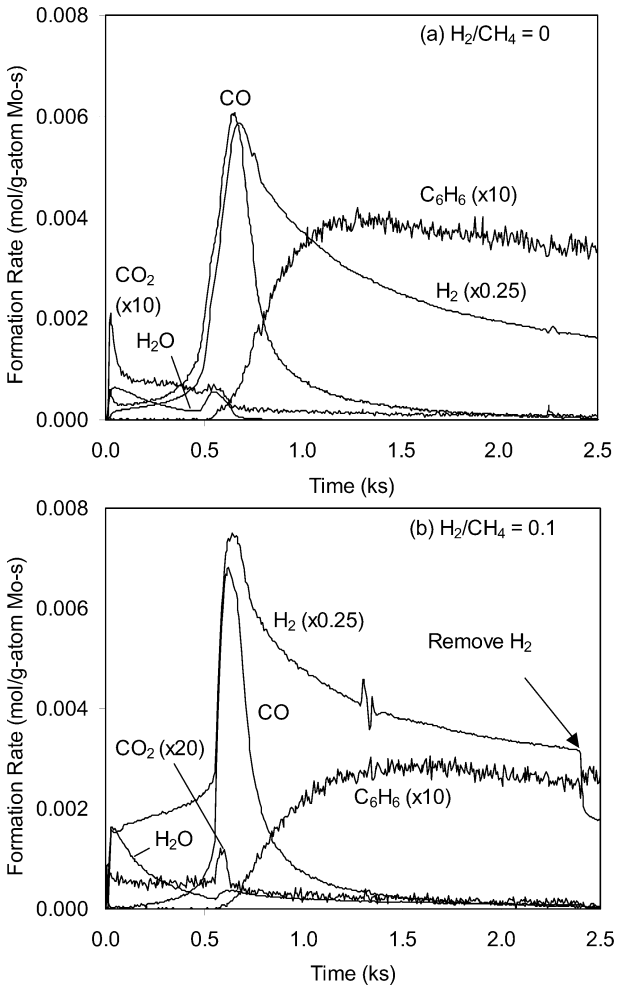

Fig. 1 Product formation during activation of $(Mo_2O_5)^{2+}$–ZSM-5 ($Mo/Al_f = 0.41$), 950 K, 18 kPa CH_4, 2 kPa Ar, balance He and total pressure of 101.3 kPa with feeds containing (a) CH_4 only and (b) a mixture with a H_2/CH_4 ratio of 0.1.

Two distinct oxygen removal regions are apparent in Fig. 1a. Initially, oxygen was predominately removed as CO and H_2O, and reduction rates showed a shallow maximum. At longer times, oxygen removal rates increased sharply in a second region, within which reduction occurs with CO as the predominant oxygen carrier (6×10^{-3} mol g-atom Mo^{-1} s^{-1} at peak) and with H_2O (5×10^{-4} mol g-atom Mo^{-1} s^{-1}) and CO_2 (5×10^{-5} mol g-atom Mo^{-1} s^{-1}) as minority reduction products. It is within this second oxygen removal region that hydrocarbon formation rates increased sharply and catalytic pyrolysis ultimately reached steady-state rates and selectivities. In the next section, each of the reduction products will be considered independently by adding them individually to CH_4 reactants.

3.2 Effects of chemical composition of reactant streams on activation and catalytic rates

Dihydrogen formation rates were significantly greater than those of any other products during the induction period (Fig. 1a). Chemisorbed hydrogen and dihydrogen formed *via* C–H bond activation of CH_4 may reduce $(Mo_2O_5)^{2+}$–ZSM-5 structures at the prevalent reaction temperatures; as the fraction of carburized Mo increases, hydrogen may spillover and reduce any remaining exchanged dimers.[25,26] The effects of H_2 on activation rates were examined using H_2/CH_4 (0.1 molar ratio) reactants at 18 kPa CH_4 and 950 K (Fig. 1b). H_2O was the only product detected during initial contact and its initial formation rate was higher than with pure CH_4 reactants, but similar to the combined rate of oxygen removal as CO and H_2O rates observed with pure CH_4. It seems likely that a minority MoO_x phase in the form of unexchanged MoO_3 clusters is also present, especially at the relatively high Mo contents ($Mo/Al_f = 0.41$) in this sample.[12] H_2O formation rates decreased with time, while CO formation rates increased sharply to a value of 6.5×10^{-3} mol g-atom Mo^{-1} s^{-1} and then decreased sharply.

As in the case of pure CH_4 reactants, two distinct reduction regions are apparent; the first peak occurs immediately after exposure to reductants but without concurrent hydrocarbon formation, while the second larger peak consists primarily of CO and appears concurrently with catalytic conversion products. Benzene first appeared after $\sim$600 s and reached a maximum rate of 2.8×10^{-4} mol C_6H_6 g-atom Mo^{-1} s^{-1}, a value slightly lower than with pure CH_4 reactants (4.0×10^{-4} mol C_6H_6 g-atom Mo^{-1} s^{-1}), because H_2 affects reverse reactions as benzene formation approaches equilibrium. When forward rates are calculated for each reactant from their net rates and respective approach to equilibrium (Table 1), the two reactant mixtures gave similar benzene formation rates (5×10^{-4} mol C_6H_6 g-atom Mo^{-1} s^{-1}). These purely thermodynamic effects of H_2 on net rates were confirmed by removing the H_2 after the induction period (Fig. 1b and Table 1). This lead to an increase in net benzene formation rate from 2.3×10^{-4} mol C_6H_6 g-atom Mo^{-1} s^{-1} to 2.9×10^{-4} mol C_6H_6 g-atom Mo^{-1} s^{-1}, while calculated forward rates remained unchanged at 3.3×10^{-4} mol C_6H_6 g-atom Mo^{-1} s^{-1} by the removal of H_2 from the reactant stream. These forward rates are slightly lower than those reported earlier in this paragraph merely because of intervening deactivation. These data show that H_2 does not influence the nature of the activation processes or the ultimate dispersion, structure, and catalytic properties of the MoC_x clusters formed from $(Mo_2O_5)^{2+}$–ZSM-5 precursors during CH_4 reactions.

C_2H_4/CH_4 mixtures were used to probe the effects of pyrolysis products, as they form during activation, on the evolution of active structures from $(Mo_2O_5)^{2+}$–ZSM-5 during catalytic reactions. Carbide formation rates were previously examined using various carburizing agents;[27–29] Xiao *et al.*[20] formed different crystalline phases of Mo_2C from MoO_3 using

Table 1 C_6H_6 formation rates in 18 kPa CH_4, 2 kPa Ar, balance He and 101.3 kPa total pressure at 950 K with different CO and H_2 feed conditions

Feed conditions (CH_4 : Ar : He : H_2)	Mo/Al_f	10^4 × Net rate[a]/mol g-atom Mo^{-1} s^{-1}	$\eta_{benzene}$	10^4 × Forward rate/mol g-atom Mo^{-1} s^{-1}
9 : 1 : 45 : 0	0.41	4.0	0.25	5.3
9 : 1 : 45 : 0	0.25	4.1	0.24	5.4
9 : 1 : 44.1 : 0.9	0.41	2.8	0.44	5.0
9 : 1 : 45 : 0[b]	0.25	3.7	0.26	5.0
9 : 1 : 45 : 0[c]	0.25	3.8	0.28	5.3
9 : 1 : 44.1 : 0.9[d]	0.41	2.3	0.30	3.3
9 : 1 : 45 : 0[e]	0.41	2.9	0.13	3.3

[a] Measurement uncertainty is 1×10^{-5} mol g-atom Mo^{-1} s^{-1}. [b] Pretreated in 7% CO/He for 0.5 h prior to carburizing in CH_4. [c] Pretreated in 7% H_2/He for 0.5 h prior to carburizing in CH_4. [d] Measured immediately before H_2 removed from feed (Fig. 1b). [e] Measured immediately after H_2 removed from feed (Fig. 1b).

temperature-programmed reaction of H_2 with various C_1–C_4 species and reported a higher reactivity with increasing hydrocarbon chain size. To our knowledge, however, isothermal carburization dynamics have not been examined for these materials. We have measured activation rates of $(Mo_2O_5)^{2+}$–ZSM-5 using streams with two C_2H_4/CH_4 molar ratios (0.005 and 0.1). Net benzene formation rates were higher when C_2H_4 was present along with CH_4 reactants, because its direct conversion to hydrocarbons is much faster than CH_4 conversion to higher hydrocarbons on acid sites; these acid sites are available even before activation of Mo-oxo precursors. C_2H_4 conversion pathways on acid sites are assisted by hydrogen desorption on MoC_x clusters and become faster as oxygen removal occurs, because hydrogen desorption sites become available as MoC_x clusters form during activation.[13,30]

These fast ethene reactions prevent an accurate assessment of ethene effects on the length of the induction period required to achieve catalytic hydrocarbon synthesis. As a result, we measured instead the effects of C_2H_4 on oxygen removal rates, given by the combined formation rates of CO, H_2O and CO_2 (×2) during initial contact with CH_4–C_2H_4 mixtures (Fig. 2). C_2H_4 increased oxygen removal rates and its effect became stronger as the C_2H_4 concentration increased. This contrasts the apparent ineffectiveness of H_2 in oxygen removal. H_2O, formed within the first reduction region, appears to inhibit further $Mo_2O_5^{2+}$ reduction in CH_4 or H_2/CH_4 streams, but these effects are much weaker or absent when C_2H_4 is used in reduction–carburization processes. With C_2H_4, the two reduction regions overlap significantly and the first reduction appears as a shoulder within the second one. We cannot definitively and exclusively attribute the predominant oxygen removal process within the second region to reactions of C_2H_4. Other alkanes and alkenes formed *via* C_2H_4 reactions on acid sites, which are present even before MoO_x reduction and carburization, can act as even more reactive carburization reagents than C_2H_4; therefore, the activating effect of C_2H_4 may arise from its C_{2+} reaction products. In any case, the addition of C_2H_4 clearly increases the rate of carburization of exchanged $Mo_2O_5^{2+}$. These activation enhancements are useful in decreasing the required activation temperatures not only for Mo-based materials, but even more importantly for less reducible exchanged cations such as V or W, which typically require much higher treatment temperatures than Mo-based materials.[31]

Fresh samples of $(Mo_2O_5)^{2+}$–ZSM-5 ($Mo/Al_f = 0.25$) were activated at 950 K with two different C_2H_4 concentrations to compare steady-state catalytic CH_4 conversion rates on samples activated with C_2H_4-CH_4 or pure CH_4 reactants. When benzene rates reached a maximum value, ethene was removed by replacing the reactant stream with one containing only CH_4 reactants (CH_4 : Ar : He = 9 : 1 : 45; 101.3 kPa). Forward rates of benzene formation from these CH_4 feeds are shown in Table 2. For C_2H_4/CH_4 molar ratios of 0.01, the benzene forward rate was 5.1×10^{-4} mol C_6H_6 g-atom Mo^{-1} s^{-1}; this is similar to rates on catalysts activated with pure CH_4 reactants (5.4×10^{-4} mol C_6H_6 g-atom Mo^{-1} s^{-1}). At higher ethene concentrations ($C_2H_4/CH_4 = 0.10$), the catalyst was rapidly reduced, but resulting forward benzene formation rates from CH_4 were considerably lower (2.3×10^{-4} mol C_6H_6 g-atom Mo^{-1} s^{-1}), apparently because rapid Mo reduction leads to poorly dispersed carbide clusters. Alternatively, this may reflect overcarburization and encapsulation of MoC_x clusters caused by unreactive deposits formed *via* reactions of C_2H_4 or its products. Previous studies showed that H_2 can remove amorphous carbon species that can block access to Mo[32,33] and W[34] carbide surfaces. Thus, the sample exposed to $C_2H_4/CH_4 = 0.10$ was heated from ambient temperature to 950 K at 0.167 Ks^{-1} in 7% H_2/He and held at 950 K for 0.5 h. The sample was then flushed with He and the CH_4/Ar/He reactants were reintroduced. Benzene formation rates were 5.1×10^{-4} mol C_6H_6 g^{-1} (atom Mo)$^{-1}$ s^{-1}, in excellent agreement with rates measured on $(Mo_2O_5)^{2+}$–ZSM-5 after alternate activation protocols. Therefore, feeds with high C_2H_4 can be used for rapid activation of reducible cation exchanged H–ZSM-5 without

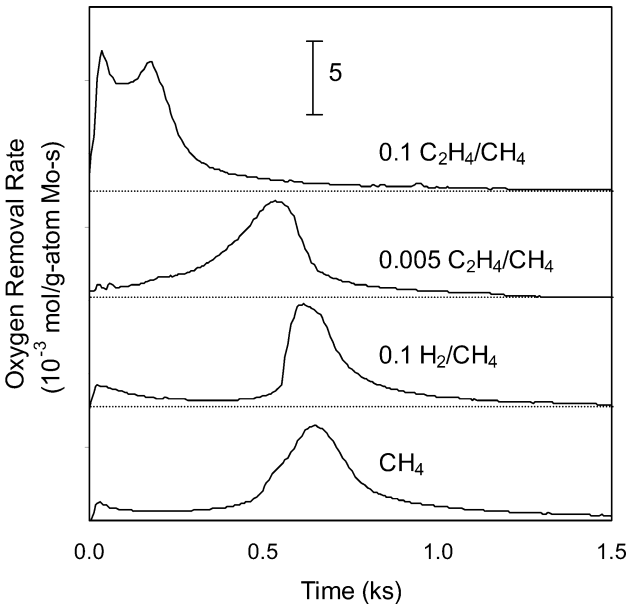

Fig. 2 Oxygen removal rates during activation of $(Mo_2O_5)^{2+}$–ZSM-5 ($Mo/Al_f = 0.41$), 950 K, 18 kPa CH_4, 2 kPa Ar, balance He and total pressure of 101.3 kPa with different co-reactants.

Table 2 C_6H_6 formation rates on Mo–ZSM-5 ($Mo/Al_f = 0.25$) in 18 kPa CH_4, 2 kPa Ar, 81 kPa He after induction at 950 K with different C_2H_4 feed conditions

Induction conditions (CH_4 : Ar : He : C_2H_4)	10^4 × Net rate[a]/mol g-atom Mo^{-1} s^{-1}	$\eta_{benzene}$	(10^4 × Forward rate/mol g-atom Mo^{-1} s^{-1}
9 : 1 : 45 : 0	4.1	0.24	5.4
9 : 1 : 44.9 : 0.1	3.9	0.23	5.1
9 : 1 : 44.1 : 0.9	2.0	0.11	2.3
9 : 1 : 45 : 0[b]	4.1	0.20	5.1

[a] Measurement uncertainty is 1×10^{-5} mol g-atom Mo^{-1} s^{-1}. [b] Measured after H_2 TPR of catalyst treated with $C_2H_4/CH_4 = 0.1$.

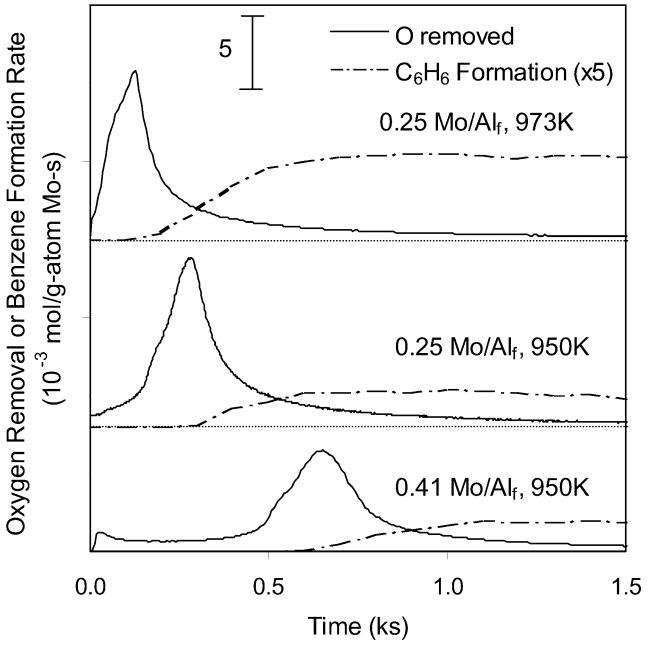

Fig. 3 O-atom removal rate and benzene formation as a function of time during activation of $(Mo_2O_5)^{2+}$–ZSM-5 (0.25–0.41 Mo/Al_f), 950–973 K, 18 kPa CH_4, 2 kPa Ar, 81 kPa He. O-atom removal rates are the sum of CO, H_2O and twice CO_2.

losses in activity. Primary activation in C_2H_4 led to excess carbon deposition and lower pyrolysis rates, but these lower rates were not caused by lower MoC_x dispersion, because pyrolysis rates became similar to those on samples activated in pure CH_4 reactants after a H_2 treatment was used to remove excess carbon.

The relatively high Mo/Al_f ratios in this sample (Mo/Al_f = 0.41) can lead to residual unexchanged MoO_3 clusters, which reduce more easily than exchanged dimers and give rise to the first reduction peak observed during activation in CH_4 and H_2/CH_4 streams. Al_f distributions in ZSM-5 with varying Si/Al_f ratios modeled by Rice *et al.*[35] and estimates of the size of Mo oxo-dimers from X-ray absorption fine structure analysis led Li *et al.*[12] to develop criteria for the maximum exchange capacity for Mo-oxo dimers in ZSM-5. For the Si/Al_f atomic ratio in our samples ($\sim$20), the maximum exchange capacity is achieved at Mo/Al_f ratios of $\sim$0.4, similar to that in this sample. Lower Mo/Al_f ratios would minimize unexchanged MoO_3 clusters; as a result, the first reduction peak should decrease in intensity and possibly disappear if it reflects oxygen removal from unexchanged MoO_3 clusters. Also, this second stage may occur earlier when MoO_3 clusters are not present if H_2O formed during its reduction inhibits subsequent reduction-carburization processes.

These hypotheses were examined using samples with a Mo/Al_f atomic ratio of 0.25 and measuring their activation and steady-state behavior in CH_4 streams. Indeed, only one reduction stage was observed (Fig. 3). Benzene first appeared earlier on this sample than on the sample with the higher Mo/Al_f ratio (320 s *vs.* 600 s), as expected if H_2O formed during the first reduction peak inhibited reduction and carburization of MoO_x precursors farther along the catalyst bed. Not surprisingly, the treatment temperature also influenced the induction time required with benzene first detected after only 200 s at 973 K.

These results indicate that C_2H_4 (or its reaction products) in CH_4 reactants increases activation rates without affecting the dispersion or reactivity of carburized $(Mo_2O_5)^{2+}$–ZSM-5, while H_2 does not influence activation rates or catalytic performance of the resulting MoC_x species. Pre-reduction with CO at 1023 K did not influence the carburization processes and catalytic properties of MoO_x–ZSM-5 precursors,[9] but led to significant CH_4 conversion rate enhancements for other exchanged precursors (Fe, V, Cr). We have found no previous quantitative transient studies of isothermal activation and catalytic evolution of cation-exchanged zeolites pre-treated in CO or H_2 before contact with CH_4. Therefore, $(Mo_2O_5)^{2+}$–ZSM-5 (Mo/Al_f = 0.25) materials were treated in 7% CO/He or 7% H_2/He streams at 950 K for 0.5 h and then exposed to 18% CH_4/Ar/He while continuously monitoring the effluent stream (Fig. 4) to determine activation rates after various pretreatment protocols. CO_2 was formed by reduction of Mo(VI)-oxo species during CO treatment (Fig. 4a). The amount of oxygen removed as CO_2 was 0.6 O/Mo during this CO treatment, while the remaining O-atoms were removed during subsequent exposure to CH_4 reactants. CO cannot replace Mo at the exchange sites because CO, in contrast with H_2, cannot provide the required charge balancing cation for exchange sites. The combined number of O-atoms removed is consistent with $Mo(V)O_2^+$ converted to active MoC_x. Benzene was formed immediately after CO was replaced with CH_4 and increased to a maximum rate of 5.1×10^{-4} mol C_6H_6 g-atom Mo^{-1} s^{-1}, slightly lower than the rate on CH_4 activated catalysts (5.4×10^{-4} mol C_6H_6 g-atom Mo^{-1} s^{-1}).

Exposure of exchanged precursors to H_2 at 950 K (Fig. 4b) led to the immediate evolution of H_2O, the rate of formation of which decreased with time. Table 3 shows the total amount of oxygen containing species removed with the various reactant and pre-treatment streams. The amount of oxygen removed after 0.5 h was $\sim$1 O-atom per Mo, corresponding to a two-electron reduction of Mo^{6+} to Mo^{4+}. Oxygen removal rates increased sharply when H_2 was replaced by the CH_4-containing stream and CO became the predominant reduction product. The appearance of benzene occurred much earlier (80 s) than on the same sample exposed to CH_4 without previous treatment in H_2 ($\sim$600 s). In contrast, benzene formation was detected immediately upon exposure to CH_4 reactants after CO pre-reduction, even though both CO and H_2 reductants failed to remove all oxygen atoms from $Mo_2O_5^{2+}$. These differences suggest that a different oxide phase forms during treatment with CO and H_2 reductants. Unlike CO, H_2 can remove $Mo_2O_5^{2+}$ from exchange sites during reduction, leading to Mo sub-oxides and to the re-formation of zeolitic protons originally replaced by Mo-oxo dimers during exchange. The exchanged Mo(V)-oxo monomers formed during CO reduction appear to be active for CH_4 pyrolysis, while MoO_2 formed during H_2 treatment become active only after further reduction and carburization.

The formation of Mo^{4+} intermediates during carburization of MoO_3/Al_2O_3 was reported previously;[28] MoO_3 carburization in 20% CH_4/H_2 mixtures was shown to occur with initial formation of MoO_2 before the incipient formation of an oxycarbide phase, as detected by X-ray diffraction. In the present study, the removal of oxygen atoms from $Mo_2O_5^{2+}$ dimers creates coordinately unsaturated Mo centers. These Mo centers activate CH_4 to form active oxycarbide species that also catalyze CH_4 activation and complete the carburization process.[36–39] The remaining 1.5 O-atoms per Mo were removed during subsequent contact with CH_4. Benzene forward rates on H_2 pre-reduced $(Mo_2O_5)^{2+}$–ZSM-5 are 5.3×10^{-4} mol C_6H_6 g-atom Mo^{-1} s^{-1} (Table 1), similar to catalysts activated in different methane mixtures and suggesting that carbide clusters formed after H_2 treatment resemble in structure and reactivity those formed during activation in pure CH_4 or CH_4–H_2 and CH_4-C_2H_4 mixtures.

The number of residual O-atoms removed (per Mo-atom) was measured as a function of time by integrating product formation rate profiles for all O-containing products and each reactant mixture; these data are shown as residual O-atoms per Mo in Fig. 5. With all reactant mixtures, a total of 2.54 ± 0.05 O-atoms per Mo atom were ultimately removed (for Mo/Al_f = 0.41), consistent with the complete reduction of exchanged $(Mo_2O_5)^{2+}$ dimers; this value was similar (2.50 ± 0.05 O-atoms

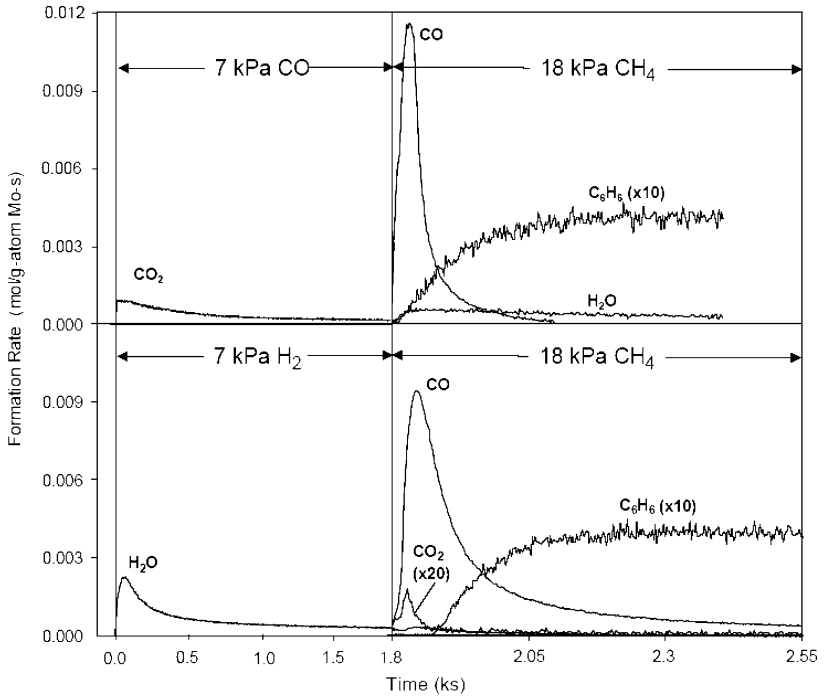

Fig. 4 Product formation during activation of $(Mo_2O_5)^{2+}$–ZSM-5 ($Mo/Al_f = 0.25$), 950 K, in (a) 7 kPa CO/94 kPa He followed by treatment in 18 kPa CH_4/2 kPa Ar/81 kPa He and (b) 7 kPa H_2/94 kPa He followed by treatment in 18 kPa CH_4/2 kPa Ar/81 kPa He. At 1.8 ks, the feed is changed from CO or H_2 to CH_4 containing mixtures.

removed per Mo atom) to that for the sample with a Mo/Al_f ratio of 0.25. The small excess of O atoms removed arising from unexchanged MoO_3 is consistent with the observed first peak in Fig. 1. We estimate by calculating the total O-atoms removed during the first reduction peak that unexchanged MoO_3 represented approximately 8% of all oxygen atoms removed.

C_6H_6 and other hydrocarbon products were first detected when residual O/Mo ratios reached values of $\sim$0.6 with both CH_4 and H_2/CH_4 feeds (Fig. 5). With C_2H_4-CH_4 mixtures, the $O_{removed}/Mo$ ratio was too low to be detected (Fig. 5) when benzene first appeared, because ethene forms benzene and other hydrocarbons *via* acid-catalyzed oligomerization reactions that do not require MoC_x sites. Benzene rates rapidly increased after initial contact with C_2H_4/CH_4 reactants as a result of MoC_x sites formed that are more active than $Mo_2O_5^{2+}$. Benzene forward rates are shown in Fig. 6 as a function of the number of O-atoms removed per Mo with C_2H_4/CH_4 (0.1) reactants. Initial benzene formation rates were 2.6×10^{-4} mol C_6H_6 g-atom Mo^{-1} s^{-1} for $O_{removed}/Mo$ below 0.25 and increased to 6×10^{-4} mol C_6H_6 g-atom Mo^{-1} s^{-1} at 0.5 $O_{removed}/Mo$. Benzene rates slightly decreased at contact times corresponding to the appearance of H_2O during the first

Table 3 O-atoms removed by different reduction products in 18 kPa CH_4, 2 kPa Ar, balance He and 101.3 kPa total pressure at 950 K with different co-reactants

	O-atoms per Mo removed as each product[a]				
Mo/Al_f	H_2O[b]	CO	H_2O	CO_2	Total
0.41	—	2.09	0.28	0.08	2.53
0.41[c]	—	1.76	0.66	0.08	2.58
0.25	—	2.27	0.18	0.03	2.51
0.25[d]	1.11	1.34	0.05	0.01	2.50
0.41[d]	1.22	—	—	—	—

[a] Uncertainty is 0.05 mol per Mo. [b] H_2O formed during pre-reduction only. [c] Activated in a mixture with H_2/CH_4 ratio of 0.1. [d] Sample pre-reduced in H_2 but not exposed to CH_4.

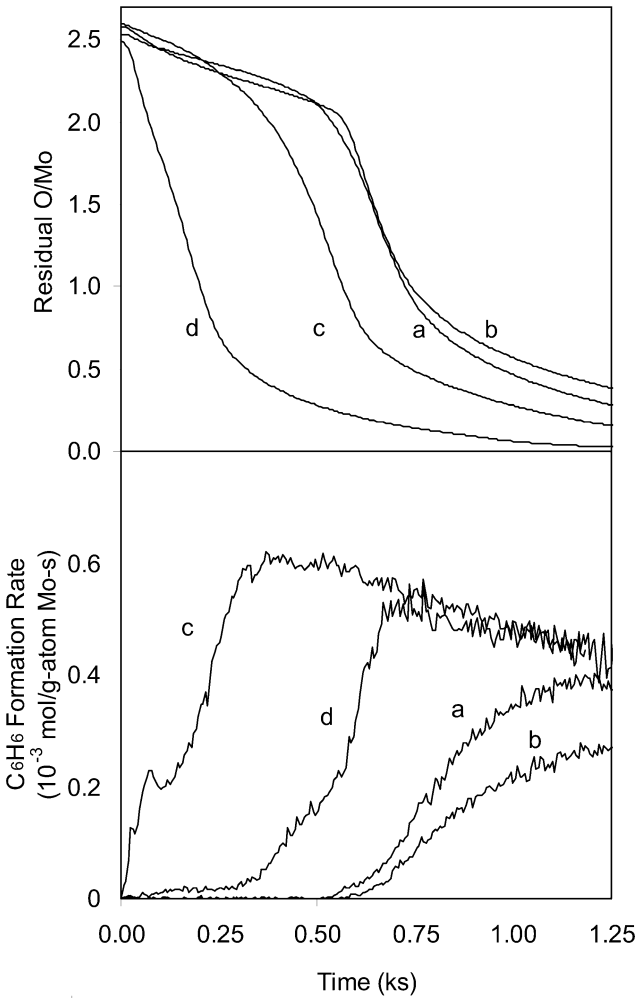

Fig. 5 Residual oxygen atoms per Mo atom (top) during activation of $(Mo_2O_5)^{2+}$–ZSM-5 ($Mo/Al_f = 0.41$), 950 K, 18 kPa CH_4, 2 kPa Ar, balance He and total pressure of 101.3 kPa with feed containing (a) CH_4 only, (b) a mixture with a H_2/CH_4 ratio of 0.1, and mixtures with C_2H_4/CH_4 ratios of (c) 0.005 and (d) 0.1. C_6H_6 formation rates are in bottom panel.

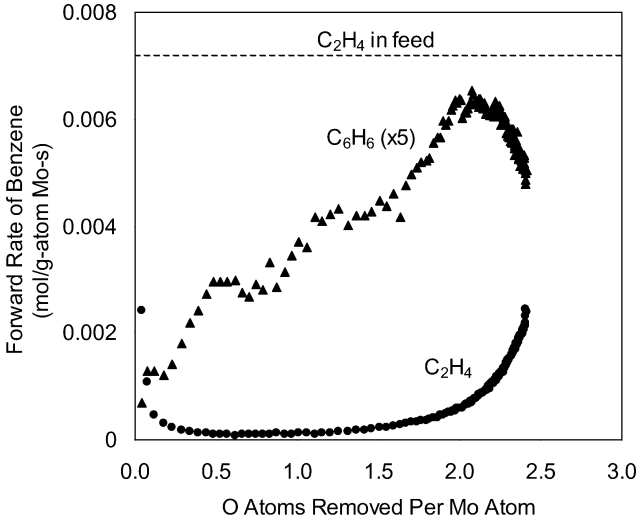

Fig. 6 Unreacted ethene and benzene formation *vs.* O/Mo removed during activation of $(Mo_2O_5)^{2+}$–ZSM-5 ($Mo/Al_f = 0.41$), 950 K, 18 kPa CH_4, 2 kPa Ar, balance He and total pressure of 101.3 kPa ($C_2H_4/CH_4 = 0.1$).

reduction peak. Benzene rates then increased monotonically above $O_{removed}/Mo$ ratios of 0.75 to a maximum of 1.3×10^{-3} mol C_6H_6 g-atom Mo^{-1} s^{-1}, and ultimately decreased slowly with time as a result of deactivation. Ethene conversion increased during the early stages of reduction, between an $O_{removed}/Mo$ ratio of 0 to 0.5, and was almost 100% converted during latter stages of carburization. This initial increase in C_2H_4 conversion also appears to be related to active carbide or oxycarbide formation, which act to remove hydrogen as H_2 during dehydrogenation reactions required for alkene conversion to aromatics.[40,41]

The effects of H_2O and CO_2 on activation rates of MoO_x precursors were examined by adding controlled amounts of these species to CH_4 reactants. CO formation rates during activation are shown in Fig. 7 for H_2O partial pressures of 0 and 0.5 kPa and for CO_2 partial pressures of 0 and 0.7 kPa at 950 K and 18 kPa CH_4. With 0.5 kPa H_2O, the first reduction peak was similar to that in water-free reactant streams, but no further reduction or formation of hydrocarbons was detected. Reduction occurred, along with a sharp increase in CO formation rates, immediately upon removal of H_2O from the reactant stream. CO_2 was also found to inhibit activation; at 0.7 kPa CO_2, there was complete inhibition of reduction. Activation occurred only after the removal of CO_2 from the feed and benzene synthesis rates reached values similar to those obtained on samples activated with pure CH_4 reactants (5×10^{-4} mol C_6H_6 g-atom Mo^{-1} s^{-1}). Similar inhibition effects with H_2O are also evident from the data shown in Fig. 7. After H_2O removal from the reactant stream at 1.2 ks, CO evolution occurred rapidly, but with a profile very different from those observed with other reactant mixtures (see Fig. 1). Incipient reduction occurred slowly immediately upon H_2O removal, because residual H_2O concentrations decreased as the H_2O-free stream gradually swept the reactor and the transfer lines and carburization rates concurrently increased. These H_2O effects on carburization dynamics suggest that space velocity and CH_4 reactant pressure also influence induction periods and activation rates, because of concomitant effects on the prevalent water concentrations.

H_2O inhibition also occurred when H_2O formed *via* reduction of $Mo_2O_5^{2+}$ with CH_4 or H_2-CH_4. In CH_4 (Fig. 1a), maximum H_2O (and CO_2) formation rates in the second reduction stage always occurred before CO formation rates reached their maximum values, apparently because reduced/carburized Mo centers become active for reforming reactions that consume both H_2O and CO_2. Moreover, H_2O and CO_2 formation inhibits further reduction, and there is an inflection point at $\sim$0.5 ks in CO formation rates as a consequence of water inhibition. As H_2O and CO_2 formation decreases, there is another inflection in the CO rate ($\sim$0.6 ks) as inhibition by these oxidants decreases. The decrease in H_2O and CO_2 oxidant formation rates reflects the stoichiometric depletion of MoO_x species as well as the reforming of CH_4 by H_2O and CO_2 as active MoC_x clusters start to form.

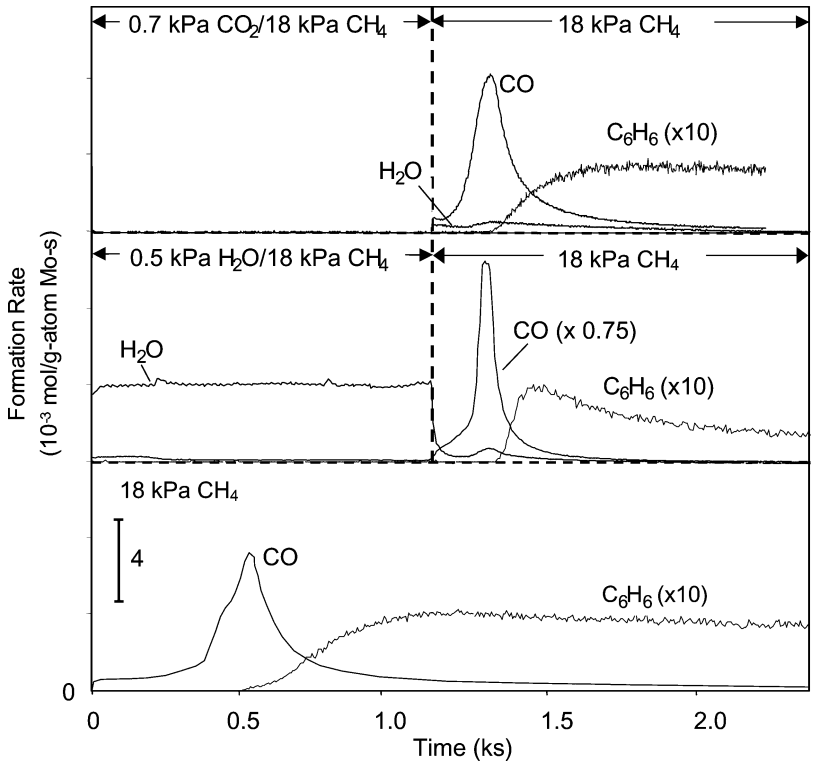

Fig. 7 CO formation rates during activation of $(Mo_2O_5)^{2+}$–ZSM-5 ($Mo/Al_f = 0.41$), 950 K, 54 kPa CH_4, 6 kPa Ar, balance He and total pressure of 101.3 kPa with feeds containing 0–0.5 kPa H_2O or 0.7 kPa CO_2.

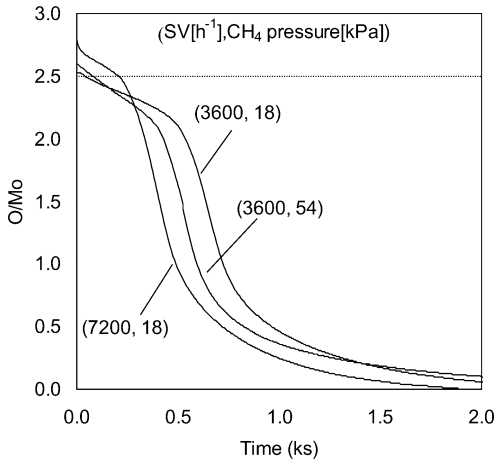

Fig. 8 Oxygen atoms removed per Mo atom during activation of $(Mo_2O_5)^{2+}$–ZSM-5 ($Mo/Al_f = 0.41$), 950 K with varying space velocity and CH_4 partial pressure.

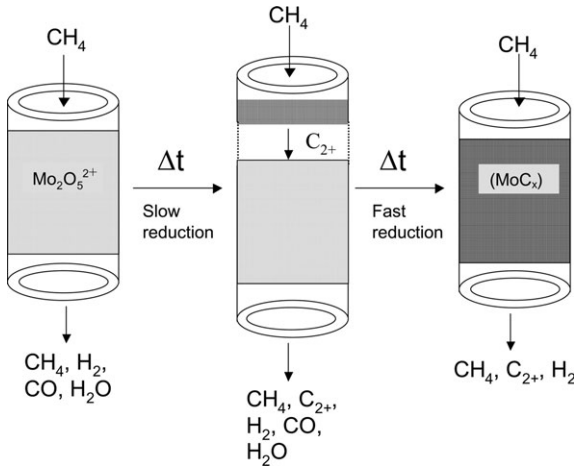

Fig. 9 Scheme for $(Mo_2O_5)^{2+}$–ZSM-5 activation in CH_4 in a plug flow reactor.

We have also examined these inhibition effects of oxidants by varying space velocity and CH_4 pressure independently. As space velocity increased, H_2O and CO_2 formed by MoO_x reduction will be removed more effectively by convection, thus decreasing their concentration and increasing activation rates. Fig. 8 shows the total O-atoms removed per Mo atom as a function of time during these activation protocols at 950 K on Mo–ZSM-5 ($Mo/Al_f = 0.41$). The baseline case (3600 h^{-1} and 18 kPa CH_4) is the same as curve *a* in Fig. 5. Higher CH_4 pressures (54 kPa) led to more rapid oxygen removal, while doubling space velocity (to 7200 h^{-1}) had an even greater effect. Increasing space velocity decreased H_2O (inhibitor) concentration, while higher CH_4 pressures increased reduction rates, but also increased H_2O and CO_x concentrations, which in turn can inhibit activation processes. H_2O and CO_2 concentration has been shown in this present study and others to effect both the rates of reduction and the stability of reduced or carburized Mo.[31,42,43] Reaction conditions which increase the H_2O or CO_2 concentration counteract those that increase reduction rates; therefore, the CH_4/H_2O ratio (and not the CH_4 or H_2O pressure independently) appear to be the critical parameter that determines activation rates. Similarly, the lack of H_2 effects on the dynamics of $Mo_2O_5^{2+}$ reduction and carburization may reflect the concurrent inhibition by the H_2O formed as H_2 incipiently reduces these Mo-oxo species.

Activation of $Mo_2O_5^{2+}$–ZSM-5 ($Mo/Al_f < 0.4$) in a tubular reactor with plug-flow hydrodynamics is shown schematically in Fig. 9. The left panel depicts the situation with fresh $(Mo_2O_5)^{2+}$–ZSM-5, which activates to form H_2, CO, CO_2 and H_2O molecules that are carried to downstream sections of the reactor. Pyrolysis products that incipiently form during this process act as reductants for $Mo_2O_5^{2+}$ species (and unexchanged MoO_3 clusters, if present) downstream and may never reach the bed outlet unreacted. The CO_2 and H_2O molecules formed inhibit further reduction and delay the onset of C_{2+} formation. As a result, reduction and carburization proceed slowly and may increase in rate as inhibitors are removed from the bed with increasing efficiency as space velocity increases. As reduction proceeds, the concentration of active MoC_x clusters increases and CH_4 yields to C_{2+} products, which act as more effective carburizing agents for downstream sections, also increase as depicted in the middle panel of Fig. 9. At this point, reduction processes accelerate because these C_{2+} products carburize remaining MoO_x precursors without apparent inhibition by co-existing water. In this manner, activation processes appear to be autocatalytic and activation rates increase until reduction and carburization approach completion (right panel in Fig. 9). After all non-framework oxygen atoms are removed, catalytic pyrolysis reactions approach their steady-state rates.

3.3 Activation of WO_x/H–ZSM-5 and VO_x/H–ZSM-5

High-valent metal oxo-cations other than $Mo_2O_5^{2+}$, such as $W(VI)O_x$ and $V(V)O_x$, can interact with Si–OH–Al sites to form anchored species in H–ZSM-5.[8,10] $W(VI)O_x$–ZSM-5 reduces and carburizes in CH_4 at 973 K to form an active pyrolysis catalyst, but reduction processes occur slower than on $Mo_2O_5^{2+}$–ZSM-5 and with lower resulting pyrolysis rates.[10] Here, we extend the activation protocols described above for Mo-based materials by exploring the use of C_2H_4/CH_4 mixtures to decrease activation periods and possibly increase steady-state catalytic pyrolysis rates.

$W(VI)O_x$-and $V(V)O_x$–ZSM-5 (0.5 g, 0.1 $cm^3\ s^{-1}$ $W/Al_f = 0.25$, $V/Al_f = 0.2$) were first exposed to 91 kPa CH_4 at 973 K in order to measure forward benzene synthesis rates (Table 4) and induction times. Maximum benzene synthesis rates were 1.3×10^{-4} mol g-atom $W^{-1}\ s^{-1}$ on W–ZSM-5; they were achieved after an induction period of 16 ks, during which rates increased much more slowly than for Mo(VI)O precursors, because of the more refractory nature of $W(VI)O_x$ precursors.[44,45] Maximum benzene forward rates on V–ZSM-5 were lower at 3.0×10^{-5} mol g-atom $V^{-1}\ s^{-1}$ after a 4 ks induction period. Both materials demonstrated lower C_6H_6 synthesis rates than Mo–ZSM-5 (4×10^{-4} mol g-atom $Mo^{-1}\ s^{-1}$) after activation in pure CH_4, suggesting a lower reactivity, poorer dispersion, or incomplete carburization of VO_x and WO_x precursors.

Table 4 C_6H_6 formation rates on V–ZSM-5 ($V/Al_f = 0.2$) and W–ZSM-5 ($W/Al_f = 0.25$) at 973 K, 91 kPa CH_4, 10 kPa Ar

Catalyst	M/Al_f	Induction time/ks	$10^4 \times$ Forward C_6H_6 synthesis rate/mol g-atom $M^{-1}\ s^{-1}$
W–ZSM-5	0.25[a]	16	1.3
	0.25[b]	2.5[c]	1.5
V–ZSM-5	0.2[a]	4	0.3
	0.2[b]	0[c]	1.0

[a] 9 : 1 CH_4 : Ar, 0.10 $cm^3\ s^{-1}$, 0.5 g. [b] 0.33 $cm^3\ s^{-1}$; Catalysts (0.2 g) were exposed to a mixture with 0.9 : 9 : 1 C_2H_4 : CH_4 : Ar, 0.37 $cm^3\ s^{-1}$ for 0.3 ks, and then the reactor was purged with 1 $cm^3\ s^{-1}$ He for 1 h before introducing CH_4 reactants. [c] Induction time reported after pre-reduction in 0.9 : 9 : 1 C_2H_4 : CH_4 : Ar, 0.37 $cm^3\ s^{-1}$ for 0.3 ks, then purging the reactor in 1 $cm^3\ s^{-1}$ He for 1 h.

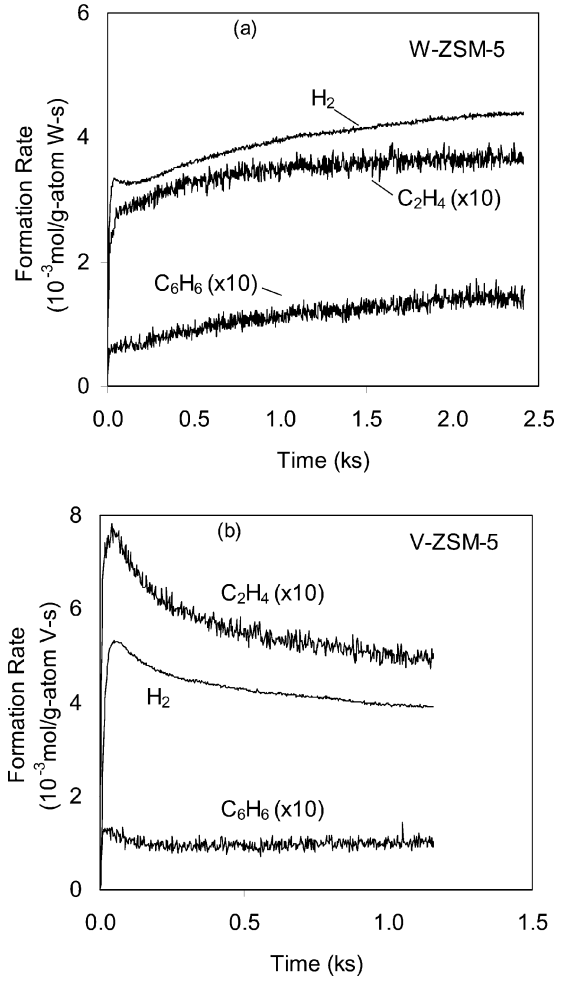

Fig. 10 CH_4 pyrolysis at 973 K, 91 kPa CH_4, 10 kPa Ar, 0.33 cm^3 s^{-1} on (a) W–ZSM-5 ($W/Al_f = 0.25$) and (b) V–ZSM-5 ($V/Al_f = 0.2$). Catalysts (0.2 g) were exposed to a mixture with 0.9 : 9 : 1 C_2H_4 : CH_4 ; Ar, 0.37 cm^3 s^{-1} for 0.3 ks, and then the reactor was purged with 1 cm^3 s^{-1} He for 1 h before introducing CH_4 reactants.

Fresh W–ZSM-5 and V–ZSM-5 samples (0.2 g) were exposed to reactant mixtures with a 0.9 : 9 : 1 C_2H_4 : CH_4 : Ar ratio (0.37 cm^3 s^{-1}) for 0.3 ks at 973 K and the reactor was then flushed with 1 cm^3 s^{-1} He for 1 h before introducing pure CH_4 reactants (0.33 cm^3 s^{-1} 91 kPa CH_4/Ar). C_6H_6 and H_2 forward rates are shown for both catalysts in Fig. 10 during exposure to this stream. C_6H_6 was immediately detected on V–ZSM-5 with a forward rate of 1×10^{-4} mol g-atom V^{-1} s^{-1}, and this rate remained constant for $\sim$1 ks. C_6H_6 also formed immediately after exposure of W–ZSM-5 to 91 kPa CH_4 with an initial forward rate of 6.0×10^{-5} mol g-atom W^{-1} s^{-1}, which increased to 1.5×10^{-4} mol g-atom W^{-1} s^{-1} after 2.5 ks time-on-stream, a value slightly higher than on W samples activated in pure CH_4 reactants (1.3×10^{-4} mol g-atom W^{-1} s^{-1}) (Table 4).

The addition of C_2H_4 to fresh catalysts either eliminated an induction period (V–ZSM-5) or significantly shortened it (W–ZSM-5). Benzene formation rates on V–ZSM-5 activated in C_2H_4/CH_4 mixtures were about threefold those measured on samples activated in pure CH_4 streams, suggesting that activation occurs more rapidly and completely when C_2H_4 is used as the carburizing agent. Benzene synthesis rates on W- and V–ZSM-5 (1.5 and 1.0×10^{-4} mol g-atom V(W) s^{-1}) were significantly lower than maximum rates on Mo–ZSM-5 (4.0×10^{-4} mol g-atom Mo^{-1} s^{-1}); however, rates on Mo–ZSM-5 decrease to levels near W- and V–ZSM-5 after $\sim$1 h exposure to reactants[10,14] to give similar performance over the catalyst lifetime.

4. Conclusion

The activation of Mo–ZSM-5 catalysts was studied by varying Mo loading and feed composition in order to study co-reactant effects on kinetics and on the length of the induction period. In samples with high Mo loadings, two reduction peaks were observed after exposure to CH_4 or mixtures of CH_4 and C_2H_4 or H_2, representing two distinct phases of Mo in the catalysts. Some of the Mo in materials with Mo/Al_f ratios above 0.41 deposited on catalyst surfaces but did not exchange. These extraframework species were easily reduced and represented the first reduction peak. The second reduction peak occurred from exchanged $Mo_2O_5^{2+}$, the predominant Mo species in these materials. In samples with Mo loadings less than 0.25, only one reduction peak was observed representing $Mo_2O_5^{2+}$ dimers bridging two cation exchange sites.

Both H_2O and CO_2 were found to completely inhibit catalyst activation at partial pressures higher than 7 kPa. H_2O and CO_2 formed initially during catalyst reduction in samples with a Mo/Al_f ratio of 0.41 inhibits further reduction of exchanged $(Mo_2O_5)^{2+}$. H_2/CH_4 mixtures were found to have no significant effect on induction period length, and this was attributed to H_2O inhibition. The addition of C_2H_4 to the feed dramatically decreased the length of the induction period and was not adversely effected by H_2O or CO_2 formation at any Mo loading.

Reduction and carburization of prevalent $Mo_2O_5^{2+}$ dimers was autocatalytic; MoC_x clusters formed initially during slow CH_4-only reduction began to convert activated CH_x surface bound species into C_2H_4 and C_{2+} intermediates. Olefin intermediates accelerated the activation process by carburizing the remaining unreduced portion of the bed until all oxygen was removed. Co-reactants such as H_2 and C_2H_4 (low concentration) changed the dynamics of activation but not the pyrolysis rates; CO_2 and H_2O, however, prevented or delayed incipient CH_4 reduction from occurring.

Pre-reduction removed a barrier to carburization by removing some of the oxygen atoms so that an oxycarbide could form without generation of H_2O or CO_2. Pre-reduction in CO, H_2 or reduction in CH_4–H_2 mixtures did not change the nature of active sites and led to product formation rates similar to those on samples activated directly in CH_4 reactant mixtures. Finally, $C_2H_4/CH_4 = 0.1$ reactant mixtures were shown to decrease or eliminate the induction period in W–ZSM-5 and V–ZSM-5, respectively, and increase benzene forward rates on V–ZSM-5 by 200%.

5. Appendix: Deconvolution of overlapping mass fragments in mass spectrum

Concentrations were determined from intensities measured by mass spectrometry using the following equations:

$$R_i = \frac{I_i}{I^*}\frac{x^*}{x_i} \qquad \text{(A1)}$$

$$x_i = \left[M_{ij}R_{ii}\right]^{-1} I_j \frac{x^*}{I^*} \qquad \text{(A2)}$$

where R_i is the mass spectrometer response factor for compound i;

I_i and I^* are the intensities of the largest fragment of species i and of the internal standard, respectively;

x_i and x^* are the mole fractions of species i and the internal standard, respectively;

$\bar{I}$ is a vector of the measured intensities I_j of each mass fragment j;

$\bar{M}$ is a matrix of the fragments, j, of compound, i, with the largest fragment of each compound normalized to unity;

$\bar{R}$ is a diagonal matrix of the response factors; $R_{ii} = R_i$;

The deconvolution method assumes the concentration of the internal standard, x^*, is constant. The molar flow rate increases during activation of $(Mo_2O_5)^{2+}$–ZSM-5, therefore it was important to operate with high concentrations of He in order to ensure accurate analysis of reactor effluent concentrations. He concentrations were greater than 80% during all experiments.

Acknowledgements

This research was funded in part by BP as part of the Berkeley-Caltech Methane Conversion Cooperative Program. Howard Lacheen acknowledges the Ford Foundation for the Ford Catalysis Fellowship of the Berkeley Catalysis Center, which he held for part of the period during which this research was conducted. The authors also acknowledge the Berkeley Catalysis Center for access to equipment used as part of this study.

References

1 J. H. Lunsford, *Catal. Today*, 2000, **63**, 165.
2 L. Chen, L. Lin, Z. Xu, X. Li and T. Zhang, *J. Catal.*, 1995, **157**, 190.
3 L. Wang, L. Tao, M. Xie and G. Xu, *Catal. Lett.*, 1993, **21**, 35.
4 S. Liu, L. Wang, R. Ohnishi and M. Ichikawa, *J. Catal.*, 1999, **181**, 175.
5 A. Szöke and F. Solymosi, *Appl. Catal. A*, 1996, **142**, 361.
6 C. D. Chang, *US Pat.* 4,273,753, 1981.
7 C. D. Chang and J. N. Miale, *US Pat.* 4,567,805, 1986.
8 B. I. Whittingtion and J. R. Andersion, *J. Phys. Chem.*, 1991, **95**, 3306.
9 B. M. Weckhuysen, D. J. Wang, M. P. Rosynek and J. H. Lunsford, *J. Catal.*, 1998, **175**, 338.
10 W. Ding, G. D. Meitzner, D. O. Marler and E. Iglesia, *J. Phys. Chem. B*, 2001, **105**, 3928.
11 F. Solymosi, J. Cserényi, A. Szöke, T. Bánsági and A. Oszkó, *J. Catal.*, 1997, **165**, 150.
12 W. Li, G. D. Meitzner, R. W. Borry and E. Iglesia, *J. Catal.*, 2000, **191**, 373.
13 R. W. Borry, Y.-H. Kim, A. Huffsmith, J. A. Reimer and E. Iglesia, *J. Phys. Chem. B*, 1999, **103**, 5787.
14 Y.-H. Kim, R. W. Borry and E. Iglesia, *Microporous Mesoporous Mater.*, 2000, **35**, 495.
15 W. Ding, S. Li, G. D. Meitzner and E. Iglesia, *J. Phys. Chem. B*, 2001, **105**, 506.
16 D. J. Wang, J. H. Lunsford and M. P. Rosynek, *J. Catal.*, 1997, **169**, 347.
17 D. R. Lide, *CRC Handbook of Chemistry and Physics*, 75th edn., CRC Press Inc, Boca Raton, 1994.
18 D. Ma, Y. Shu, M. Cheng, Y. Xu and X. Bao, *J. Catal.*, 2000, **194**, 105.
19 V. T. T. Ha, L. V. Tiep, P. Meriaudeau and C. Naccache, *J. Mol. Catal.*, 2002, **181**, 283.
20 T. Xiao, A. P. E. York, K. S. Coleman, J. B. Claridge, J. Sloan, J. Charnock and M. L. H. Green, *J. Mater. Chem.*, 2001, **11**, 3094.
21 M. Boudart and G. Djega-Mariadassou, *Kinetics of Heterogeneous Catalytic Reactions*, Princeton University Press, Princeton, NJ, 1984.
22 D. Wang, J. H. Lunsford and M. P. Rosynek, *Top. Catal.*, 1996, **3**, 289.
23 A. Holmen, O. Olsvik and O. A. Rokstad, *Fuel Process. Tech.*, 1995, **42**, 249.
24 B. M. Weckhuysen, M. P. Rosynek and J. H. Lunsford, *Catal. Lett.*, 1998, **52**, 31.
25 J. G. Kim and J. R. Regalbuto, *J. Catal.*, 1993, **139**, 175.
26 J. G. Kim, J. Z. Shyu and J. R. Regalbuto, *J. Catal.*, 1993, **139**, 153.
27 S. T. Oyama, P. Delporte, C. Pham-Huu and M. J. Ledoux, *Chem. Lett.*, 1997, 949.
28 A. Hanif, T. Xiao, A. P. E. York, J. Sloan and M. L. H. Green, *Chem. Mater.*, 2002, **14**, 1009.
29 J. B. Claridge, A. P. E. York, A. J. Brungs and M. L. H. Green, *Chem. Mater.*, 2000, **12**, 132.
30 F. Solymosi and A. Szöke, *Stud. Surf. Sci. Catal.*, 1998, **119** 355.
31 R. Ohnishi, S. Liu, Q. Dong, L. Wang and M. Ichikawa, *J. Catal.*, 1999, **182**, 92.
32 L. Volpe and M. Boudart, *J. Solid State Chem.*, 1985, **59**, 348.
33 R. Ohnishi, R. Kojima, Y. Shu, H. Ma and M. Ichikawa, *Stud. Surf. Sci. Catal.*, 2004, **147**, 553.
34 J. S. Lee, L. Volpe, F. H. Ribeiro and M. Boudart, *J. Catal.*, 1988, **112**, 44.
35 M. J. Rice, A. K. Chakraborty and A. T. Bell, *J. Catal.*, 2000, **194**, 278.
36 D. C. LaMont, A. J. Gilligan, A. R. S. Darujati, A. S. Chellappa and W. J. Thomson, *App. Catal. A*, 2003, **255**, 239.
37 A. P. E. York, J. B. Claridge, A. J. Brungs, S. C. Tsang and M. L. H. Green, *Chem. Commun.*, 1997, 39.
38 A. J. Brungs, A. P. E. York, J. B. Claridge, C. M. Alvarez and M. L. H. Green, *Catal. Lett.*, 2000, **70**, 117.
39 J. B. Claridge, A. P. E. York, A. J. Brungs, C. Marquez-Alvarez, J. Sloan, S. C. Tsang and M. L. H. Green, *J. Catal.*, 1998, **180**, 85.
40 B. Frühberger and J. G. Chen, *J. Am. Chem. Soc.*, 1996, **118**, 11599.
41 N. Liu, S. A. Rykov and J. G. Chen, *Surf. Sci.*, 2001, **487**, 107.
42 P. Ratnasamy, A. V. Ramaswamy, K. Banerjee, D. K. Sharma and N. Ray, *J. Catal.*, 1975, **38**, 19.
43 P. Arnoldy, J. C. M. de Jong and J. A. Moulijn, *J. Phys. Chem.*, 1985, **89**, 4517.
44 S. T. Oyama, *Catal. Today*, 1992, **15**, 179.
45 R. Kapoor and S. T. Oyama, *J. Solid State Chem.*, 1995, **120**, 320.